Colloid & Polymer Science Colloid Polym Sci 272:1380–1387 (1994)

The interface between immiscible polymers in composite latexes: a small-angle x-ray scattering study employing contrast variation*)

N. Dingenouts, Y. S. Kim, and M. Ballauff

Polymer-Institut, Universität Karlsruhe, Karlsruhe FRG

*) *Respectfully dedicated to Prof. E. W. Fischer on the occasion of his 65th birthday*

Abstract: An investigation of the radial structure of composite latex particles by small-angle x-ray scattering (SAXS) is given. Measurements at different contrasts were done by addition of sucrose to the dispersion medium water. The latex particles investigated here consist of a poly(styrene) core and a shell of poly(methylmethacrylate) and were prepared by seeded emulsion polymerization. Since the electron density of both polymers can be easily matched by concentrated sucrose solution, a full analysis of the radial electron density by contrast variation can be given. Depending on the mode of monomer addition during the second polymerization step a very sharp or a diffuse interface between the two incompatible polymers may result.

Key words: Small-angle x-ray scattering – latex – colloids – contrast-variation – emulsion polymerization

Introduction

Latexes composed of immiscible polymers have been studied in detail recently since these systems are of great economical and scientific interest [1–12]. An important point when discussing these systems is the width of the interface between the polymeric phases which may change as function of the different modes of particle synthesis. Using seeded emulsion polymerization the second polymer can be introduced either by polymerization under monomer-starved conditions or by the monomer-absorption method. In the first case, the second monomer is added so slowly that it is consumed almost immediately by polymerization [9, 10]. Hence, if this monomer exhibits a certain solubility in water, homogeneous nucleation in the water phase will prevail and the shell of the composite latex will be built up by adsorption of oligomeric growing chains or primary particles [13].

On the other hand, the seed latex particles may be swollen by the second monomer prior to polymerization. The homogeneous solution within the latex particle will undergo phase separation as the polymerization proceeds and polar polymers will tend to enrich at the surface [6, 7]. At a certain stage the whole system may vitrify and the structure achieved at this point will be frozen in and preserved. In this case a broad interfacial region between the two polymers may be expected.

A further complication is given by the fact that the monomer-swollen particles may already exhibit a core-shell structure in the swollen state due to the wall repulsion effect [14–17]; i.e., within the particle the monomer will be enriched near the boundary to water. A thorough study of this effect has been presented by Mills et al. [15] by small-angle neutron scattering (SANS). Employing contrast variation by use of deuterated monomers or D_2O/H_2O mixtures these authors concluded that the wall repulsion effect may be dismissed. In contrast to previous investigations [16, 17] the resulting morphology is explained by the anchoring of the growing chains onto the surface by their polar endgroups [18].

This brief survey shows clearly that the morphology of a composite latex particle may result from the balance of several effects. The understanding of these effects requires detailed knowledge of the radial structure as function of the conditions employed during polymerization.

In recent studies it could be demonstrated that small-angle x-ray scattering (SAXS) is highly suitable for the elucidation of the radial structure of composite latexes [19–21]. This is due to the fact that the rather low electron density of the polymers employed usually in emulsion polymerization can be easily matched by concentrated sucrose solution. Thus, a full study including measurements at the match point can be conducted easily over several orders of magnitude of the scattering intensity without limitations due to incoherent scattering or the necessity of using deuterated chemicals. Previous studies [20, 21] dealt with a composite latex made from poly(styrene) (PS) core particles and a poly(methylmethacrylate) (PMMA) shell which has been prepared [22] by seeded emulsion polymerization under monomer-starved conditions. Here, we present an extension of our investigations [22] on PS/PMMA composite latexes prepared by the monomer-absorption method. The radial structure as obtained by SAXS in conjunction with contrast variation will be discussed and compared to the method of polymerization. In particular, the discussion presented herein will focus on the fine structure down to a resolution of a few nanometers.

Experimental

Materials and methods

Two composite latexes consisting of poly(styrene) core (PS) and poly(methylmethacrylate) shell (PMMA) prepared in the course of a comprehensive study [22] were chosen for this investigation: Latex I termed [PSI/PMMA]-1 in reference [22] (number-average diameter: 92.3 nm) has been prepared under starved conditions using a PS core-latex with a number-average diameter of 71.5 nm; Latex II (termed [PS2/PMMA]-3 in ref [22]) was synthesized by the absorption method using a PS seed latex of 68,6 nm diameter. Its diameter was to 91.1 nm as determined by electron microscopy. In some cases the size distributions of the PS-core latex as well as of the PS/PMMA core-shell latex were determined by ultracentrifugation [23]. Further details regarding the synthesis and the characterization of the latexes used herein may be found in ref. [22].

SAXS measurements were done using a Kratky-Kompakt-Kamera (Paar, Graz, Austria) mounted on an x-ray tube with a copper anode (focal spot size: 0.4×12 mm) and equipped with a position-sensitive detector (Braun, FRG) (see ref. [21] for details). As outlined in ref. [21] the q-range accessible for this instrument ($0.08\ \text{nm}^{-1} \leq q \leq 5\ \text{nm}^{-1}$; $q = (4\pi/\lambda)\sin(\theta/2)$; θ: scattering angle) was not afflicted by the effect for interparticular interferences. Hence, measurements with this device could be conducted at rather high volume fractions (ca. 8 wt.%).

To supplement these data, several measurements were performed in the region of lower scattering angles ($0.037\ \text{nm}^{-1} \leq q \leq 0.3\ \text{nm}^{-1}$) using the step-scan device described previously [19]. The scattering data were obtained by measuring highly diluted dispersions ($\phi = 0.8$ wt.%) in order to avoid completely the effects of interparticular interferences [19].

For both cameras the intensities of the primary beam were determined using the moving slit method of Kratky and Stabinger [24]. The latex samples were confined in a Mark-capillary of 1 mm diameter thermostatted to 25 °C by means of a temperature-controller (Paar, Graz, Austria).

All data were first corrected for the effect of slit-width using the procedure of Beniaminy and Deutsch [25] and subsequently for the smearing due to the finite slit-length. For the latter correction the routine of Strobl [26] has been employed (cf. refs. [19] and [21]).

For contrast variation the electron density of the dispersion medium water was raised by adding D(+)-Sucrose (Fluka ($\geq 98\%$); used without further purification) [21]. The densities of the sucrose solution were measured using a DMA-60 apparatus (Paar, Graz, Austria). The number ρ_m of electrons/nm^3 of the sucrose solutions follows as $\rho_m = 332.79 + 1.2827 \cdot c$, where c denotes the weight percentage of sucrose in the respective solution. The sucrose was added to the stock solution and dilution was effected with 0.01 mol/l KCl-solution to achieve the same volume concentration for all contrasts.

Theory

For monodisperse particles the intensity normalized to the scattering intensity of a single electron is given by [27–29, 21]:

$$I(q) = N B^2(q) , \tag{1}$$

where N is the number of particles per unit volume and $B(q)$ is the scattering amplitude. For spherical symmetric particles with radius R, $B(q)$ is given by:

$$B(q) = 4\pi \int_0^R [\rho(r) - \rho_m] r^2 \frac{\sin(qr)}{qr} dr , \tag{2}$$

with $\rho(r)$ being the local electron density in the particles and ρ_m the respective quantity of the dispersion medium. With definition of the volume-average $\bar{\rho}$ of the electron density of the particles by

$$\bar{\rho} = \frac{4\pi \int_0^R \rho(r) r^2 dr}{4\pi \int_0^R r^2 dr} \tag{3}$$

the local density $\rho(r)$ may be rendered as

$$\rho(r) = \bar{\rho} + \Delta\rho(r) \tag{4}$$

and the scattering amplitude is split into two parts:

$$B(q) = B_0(q) + \varepsilon(q) \tag{5}$$

with

$$B_0(q) = (\bar{\rho} - \rho_m)\, 4\pi \int_0^R \frac{\sin(qr)}{qr} r^2 dr \tag{6}$$

and

$$\varepsilon(q) = 4\pi \int_0^R \Delta\rho(r) \frac{\sin(qr)}{qr} r^2 dr \tag{7}$$

For values of q satisfying $q^*R = \tan(q^*R)$ the amplitude $B_0(q)$ is zero for all constrasts and we have (cf. ref. [27–29])

$$I(q^*) = N\varepsilon^2(q) \quad q^*R = 4.4934, 7.7253\cdots \tag{8}$$

Since $\varepsilon(q)$ does not depend on contrast, all scattering intensities of uniform systems must intersect at $q = q^*$.

The radial electron density can be modeled using an expression given by Helfand and Tagami [30]:

$$\rho(r) = \rho_{\text{core}} + \frac{\rho_{\text{shell}} - \rho_{\text{core}}}{1 + \exp[c\cdot(r_0 - r)]} , \tag{9}$$

where ρ_{core} denotes the electron density of the core material PS, ρ_{shell} the respective quantity of PMMA, r_0 defines the midpoint of the interface and c is a positive constant characterizing the width of the interface. Insertion of (9) into (2) and subsequent integration leads to the scattering amplitude and the intensity through Eq. (1).

For a composite particle the final slope of the scattering curves follows from Porod's law as (cf. ref. [31])

$$I(q) \approx 2\pi N [\Delta\rho_i^2 \cdot S_i + \Delta\rho_a^2 \cdot S_a] \cdot q^{-4} + I_{\text{fluct}} , \tag{10}$$

where S_i denotes the internal surface of the particles originating from the two polymer phases; $\Delta\rho_i$ is the respective difference of the electron density. The second term refers to the outer surface S_a between the particle and the dispersant. Here, $\Delta\rho_a$ denotes the difference of the electron densities at this surface. Varying the contrast therefore allows to distinguish between these two contributions to the final slope. The last term I_{fluct} is the background due to the density fluctuations of both polymers already discussed previously [21]. In the q-range under consideration here this contribution may be assumed to be independent of q in good approximation.

For polydisperse systems the intensity follows as

$$I(q) = \sum_i N_i B_i^2(q) \tag{11}$$

where the index i refers to the type of particle under consideration. As outlined before [21] the particle size distribution of the PS cores was modeled using the result supplied by ultracentrifugation [23].

A fit of a given model for the radial distribution function (cf. Eq.(9)) can be done as follows: For a fixed ρ_m the scattering amplitude $B_i(q)$ is calculated by Eq. (2) for a given diameter. Summation of all $B_i^2(q)$ weighted by their number density N_i then leads to the normalized intensity. The overall number density of the latex particles can be either calculated from mass balance or taken as a fit parameter. In all cases the fit of the experimental

data is only acceptable if the number density obtained from the fit matches the experimental value.

Results and discussion

Latex I

The radial structure of a PS/PMMA latex prepared under starved conditions has been discussed recently [19–21]. Here, we extend this analysis in order to obtain quantitative information on the interface between the PS and the PMMA-phase. By SAXS in conjuction with contrast variation [21] it could be shown that latex I exhibits a well-defined core-shell morphology with a number-average core diameter of 74.4 nm and a PMMA-shell of an average thickness of 7.06 nm. The thickness was modeled assuming a Gaussian distribution with a standard deviation of 2.09 nm. Furthermore, it could be shown (cf. the discussion of Fig. 6 in ref. [21]) that the width of the shells is not coupled to the diameter of the cores.

The latter point can be derived immediately when looking at the small-angle region: If the thickness of the PMMA-shells is strictly proportional to the diameters of the cores, all particles will have nearly the same average electron density $\bar{\rho}$ (cf. Eq. (3)). Hence, forward scattering (cf. Eq. (6)) will vanish or at least strongly diminish at the match point which is not observed in experiment.

The foregoing discussion thus shows that important features of the structural model can be checked very accurately in the small-angle region if the measurements are done in the immediate vicinity of the match point. Since such features as, for example, polydispersity of the shells also may influence the wide-angle region, their accurate determination is of utmost importance for the quantitative determination of the width between the two polymer phases.

Having clarified the overall structure of the particles we now turn to the discussion of the interface in latex I.

Figure 1a displays the comparison of the fits of a model with a sharp interface (dashed line, see inset of Fig. 1a) and a diffuse interface. In the latter case the same core radii as used previously for modeling the sharp interface were taken as the

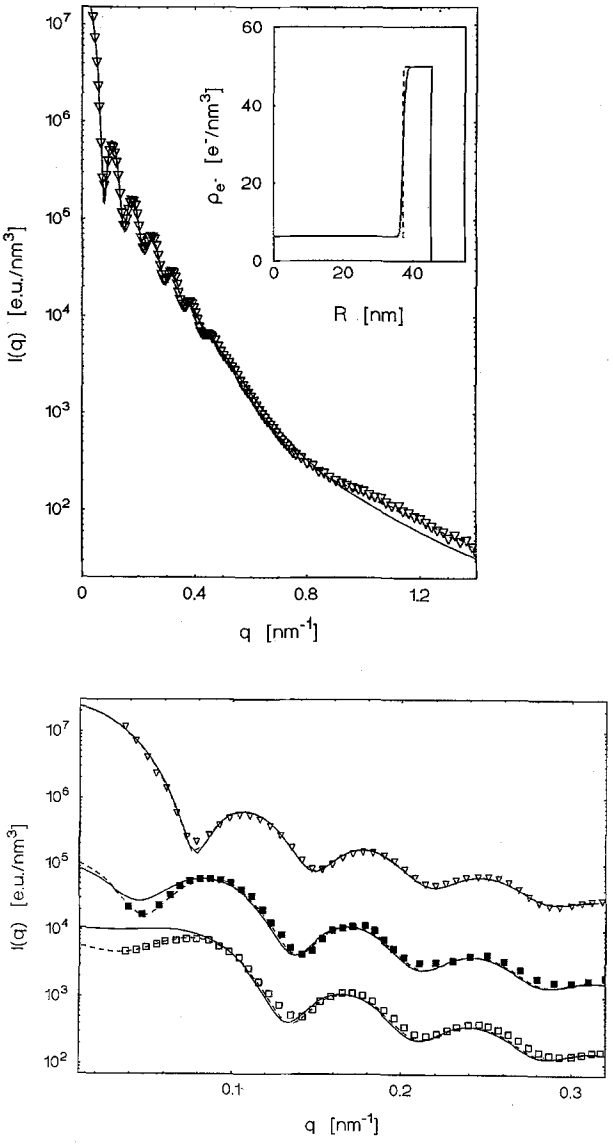

Fig. 1. Latex 1 (prepared by monomer-starved conditions): Comparison of a core-shell model with a sharp interface (dashed line) and a diffuse interface (solid line, width of the interface 4 nm) with experimental scattering intensity. Fig. 1a: q-range measured at highest contrast (in water). The inset displays the different models for the radial density; Fig. 1b: Scattering intensity in the low-q range at three different contrasts: ▽ ▽: water; ■ ■: 16% sucrose solution; □ □: 19.6% sucrose solution (match point)

radial position r_0 of the diffuse interface. The width of the interface defined through the region in which the electron density is more than 2% above its values of the core (PS) and below 98% of the respective values of the shell (PMMA) was assumed to be 4 nm. The shell of pure PMMA

was modeled assuming a Gaussian distribution of its thickness again assuming a standard deviation of 2.09 nm. Thus, the modeling of the diffuse interface proceeds exactly along the lines discussed previously [21]; only a small region in which a smooth transition from PS to PMMA takes place is put in between core and shell.

The comparison of both models is displayed in Fig. 1a. The small-angle region at different contrast is shown in Fig. 1b, whereas Fig. 1a refers to the measurement at maximum possible contrast (in water). As expected, the scattering intensity at high contrast is compatible with both models with exception of the wide-angle region. Clear discrepancies of theory and experiments, however, can be revealed already in the small-angle region at vanishing contrast (see Fig. 1b). In this region these deviations are due to an incorrect average electron density $\bar{\rho}$ (cf. Eq. (3)). In the wide-angle region the slightly diffuse interface leads to smaller intensities than observed experimentally (cf. ref. [32]).

The above analysis demonstrates that the interface between PS and PMMA in latex I must be rather small indeed; the present data are only compatible with a width below 4 nm. From this finding, one is led to conjecture that the formation of the shell must proceed via homogeneous nucleation: The polymerization of the monomeric MMA under starved conditions will start in the aqueous phase to produce PMMA oligomers or small aggregates thereof. These entities will adsorb onto the surface of the PS seed latex particles [4, 13]. Since oligomeric PMMA is already incompatible with PS, no mixing will occur at the interface and a very sharp interface between the two polymers will result.

Latex II

This system has been prepared by first swelling the PS-seed particles with monomeric MMA and subsequent polymerization. The experimental details of this procedure are described in ref. [22]. Figure 2a and b display the scattering intensities obtained from latex II at different contrast. Again there are pronounced differences when changing the contrast, but Fig. 2b demonstrates that the crossing point around $q^* \approx 0.085\ \mathrm{nm}^{-1}$ (cf. Eq. (8)) is not clearly developed as is the case for latex I. The region where this condition (Eq. (8)) is

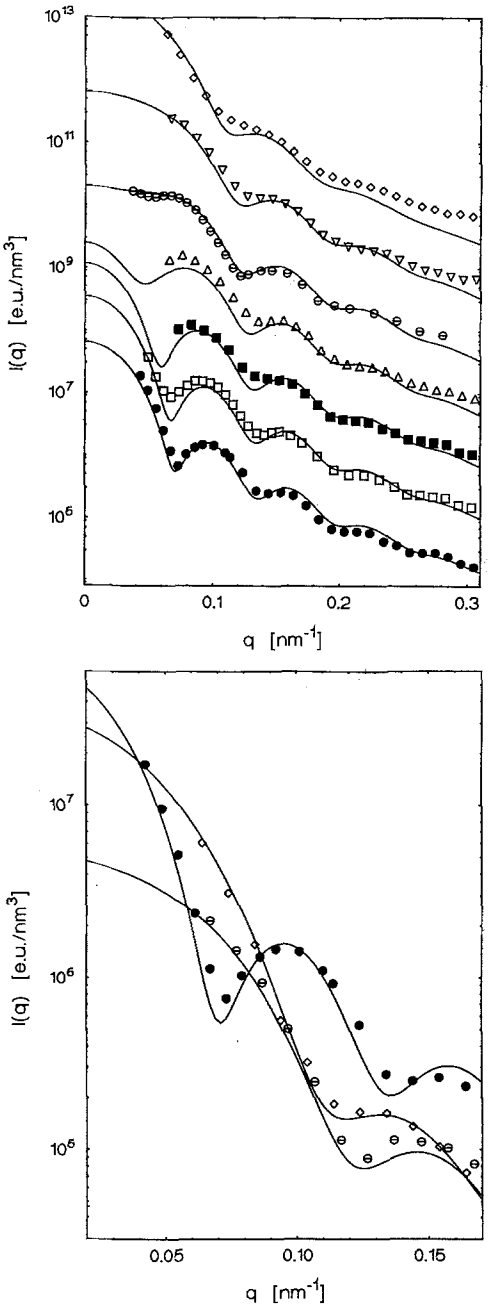

Fig. 2. Latex II (prepared by the adsorption method): Scattering intensities measured at different contrast. The solid lines present the theoretical scattering intensities calculated by assuming a diffuse interface between PS and PMMA (cf. inset of Fig. 3). Fig. 2a: $q \leq 0.4\ \mathrm{nm}^{-1}$; for the sake of clarity subsequent curves have been shifted by a factor of 10; the values at the ordinate correspond to the measurements for 0% sucrose solutions. Fig. 2b: unshifted curves at the small-angle region as measured by the step-scan device. The numbers behind the symbols refer to the weight concentration of sucrose. ● ●: 0%, □ □: 8%, ■ ■: 16%, △ △: 24%, ⊖ ⊖: 28.4% (match point), ▽ ▽: 32%, ◇ ◇: 40%

approximately fulfilled points to a diameter between 90 and 100 nm which is in agreement with the figures supplied by ultracentrifugation and electron microscopy [22].

All attempts to fit the experimental intensities by a radial electron density varying stepwise failed. The best fit for all contrasts up to $q = 0.3\ \mathrm{nm}^{-1}$ is given by the following model: There is a diffuse interface between PS and PMMA (see inset of fig. 3) with radial position r_0 and a width defined as described above (cf. Eq. (9)). The radial position r_0 as well as the width of the interfacial region is assumed to scale linearly with the outer diameter of latex II.

This is in opposition to the previous case of latex I where the thickness of the interface as well as that of the shell had to be independent of the diameter of the cores. The procedure employed for latex II is suggested by experimental studies [33] of the swelling of latex particles in which a degree of swelling independent of the size of the dry latex particles was found, i.e., the uptake of the swelling agent is proportional to the size of the particle.

In the frame of this model one obtains a number-average diameter of 92.8 nm which compares well to the value supplied by electron microscopy (91.1 nm, [22]). The standard deviation of the diameter followed as 9.0 nm and the average width of the interface as 24.7 nm from this model. The solid lines in Figs. 2a and 3 shows the good description of the experimental data by this model. Also, the overall number density of the latex taken from this fit agrees well with the experimental figure.

At higher scattering angles the fit by the above model is becoming less and less satisfying, which indicates that the fine structure is not described anymore by a smooth transition from PS to PMMA. This conclusion is borne out directly by the analysis of the final slope according to Eq. (10). Figure 4 shows that the scattering intensities at high angles ($q > 1.8^{-1}$) are described by Porod's law within experimental uncertainty. It has to be admitted, however, that in this angular region the subtraction of the background becomes increasingly different. Deviations from linearity are therefore most probable due to the low signal-to-background ratio. Also, for calculating the total surface S the overall number density of the particles has to be taken from the above fit. Therefore, the total surface obtained from Fig. 4 is subject to a considerable error. Nevertheless, Fig. 5 shows that this quantity depends approximately linearly on the square of the contrast between the shell material PMMA and the dispersion medium. Thus the contributions of the internal surface can be estimated to be twice the size expected for a sharp core-shell particle. On the other hand, if the transition from PS to

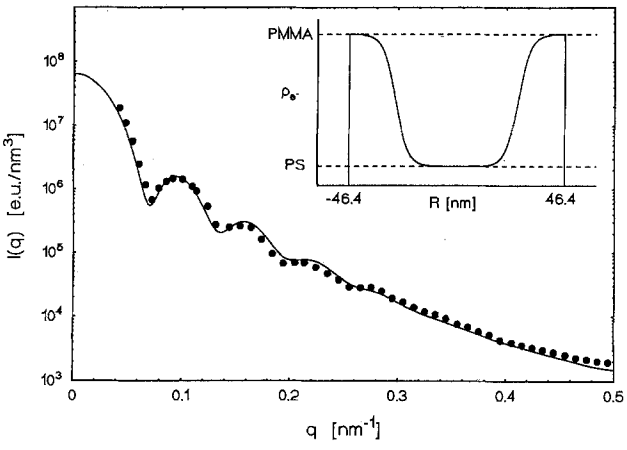

Fig. 3. Latex II: Comparison of measured (●) and calculated intensities assuming a diffuse interfacial region between the PS core and the PMMA shell. The experimental intensities refer to measurements in water

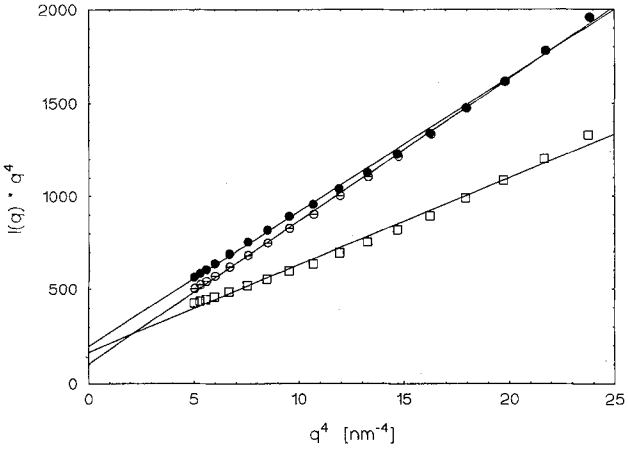

Fig. 4. Latex II: Porod plots of the experimental intensities for three different contrasts: ●●: 0%, □□: 8%, ⊖⊖: 28.4% (match point)

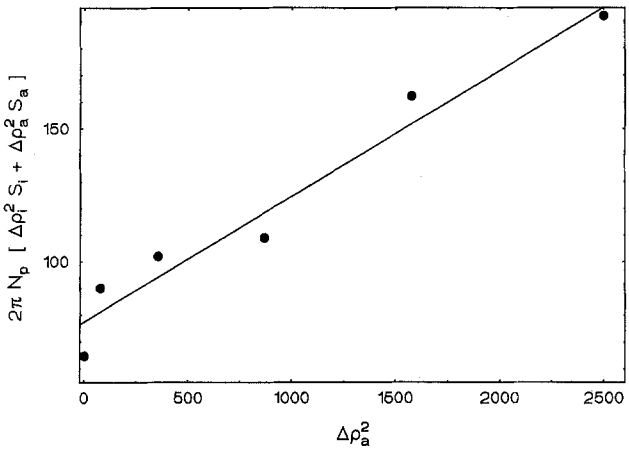

Fig. 5. Latex II: Surfaces determined by Porod plots (cf. Eq.(10) and Fig. 4) at different contrasts Δ_{ρ_a} of the sucrose solution towards the PMMA shell. At $\Delta_{\rho_a} = 0$ the contribution of the outer surface PMMA/dispersant is matched

PMMA would be mediated by an increasing number of small spheres composed of PMMA a much higher surface (at least by one order of magnitude) would result (cf. Fig. 11 in ref. [4]).

Despite the rather insecure determination of S_i by the extrapolation shown in Fig. 5 an extended internal surface can be ruled out. The SAXS-data therefore point to an intermediate structure where an irregularly shaped interface separates the PS from the PMMA phase. Averaged over all particles and orientations this structure leads to a radial electron density which is displayed in the inset of Fig. 3. On the other hand, such a model is characterized by a sharp interface between the PS and the PMMA phase when going down to a length scale of a few nanometers corresponding to the final slope of the scattering curves (cf. Fig. 4).

Besides the problems regarding the fine structure, it is clear that latex II exhibits an overall core-shell structure, i.e., most of the PMMA polymerized in the second stage is located at the periphery of the particles. Fisher et al. [34] came to the same conclusion when studying the system PS/PMMA by SANS. Also, Mills et al. [15] who polymerized deuterated PS on a protonated PS core latex through the monomer-adsorption method could demonstrate by SANS that the resulting latex particles have a pronounced core-shell structure which is explained by the surface anchoring effect. In the case of two immiscible polymers the structuring of the particles during the second step of the synthesis should be even more pronounced. The present analysis of latex II, however, can quantify the finer details of the internal structure.

It is evident that the further conclusions regarding the radial structure of latex II on the level of a few nanometers are tentative to a certain extent. This is not only due to the limitations of the scattering technique but also to the polydispersity of the size and the internal structures: The absence of a well-defined crossing point (cf. Eq. (8)) in Fig. 2b clearly demonstrates that latex II is much less uniform than latex I.

Besides these problems, when discussing the fine structure the marked difference between latex I and latex II and the influence of the polymerization process could be shown clearly. Hence, SAXS in conjunction with contrast variation is well suited to study the fine details of latex particles down to a resolution of a few nanometers.

Acknowledgement

Financial support of the Bayer AG, Geschäftsbereich Kautschuk, of the Bundesministerium für Forschung und Technologie, Pilotprojekt "Mesoskopische Systeme", and of the AIF, grant 9749, is gratefully acknowledged.

References

1. Lee DI (1990) Makromol Chem Symp 33:117
2. Okubo M (1990) Makromol Chem Symp 35/36:307
3. Lee DI, Ishikawa T (1983) J Polym Sci, Polym Chem Ed 21:147
4. Min TI, Klein A. El-Aasser MS, Vanderhoff (1983) J Polym Sci:Polym Chem Ed 21:2845
5. Paxton TR (1969) J Colloid Interf Sci 31:19
6. Okubo M, Yamada A, Matsumoto a (1980) J Polym Sci: Polym Chem Ed 16:3219
7. Cho IW, Lee KW (1985) J Appl Polym Sci 30:1903
8. Lee S, Rudin A (1989) Makromol Chem, Rapid Commun 10:655; (1992) J Polym Sci:Polym Part A:Polym Chem 30:865, 30:2211
9. Schmutzler K, Hergeth WD, Bittrich HJ, Eichhorn F, Schlenker S (1989) Polymer 60:1913, Beyer D, Lebek W, Hergeth WD, Schmutzler K (1990) Colloid Polym Sci 268:744
10. Jönsson JE, Hassander H, Jansson LH, Törnell B (1991) Macromolecules 24:126; Jönsson, JE, Hassander H, Törnell B (1994) Macromolecules 27:1932
11. Chen YC, Dimonie V, El-Aasser, MS (1991) Macromolecules 24:3779; (1992); J Appl Polym Sci 42:1049
12. Winnik MA, Zhao C-L, Shaffer O, Shivers RR (1993) Langmuir 9:2053

13. Sütterlin N, Kurth HJ, Markert G (1976) Makromol Chem 177:1549; Sütterlin N in Polymer Colloids II (Ed:Fitch RM) Plenum, New York 1978
14. Grancio MR, Williams DJ (1970) J Polym Sci Part A-1, 8:2617; Keutsch P, Price J, Williams DJ (1993) J Macromol Chem A-7:623
15. Mills MF, Gilbert RG, Napper DH, Rennie AR, Ottewill RH (1993) Macromolecules 26:3553, and further refs. cited therein
16. Yang SI, Klein A, Sperling LH, Cassassa EF (1990) Macromolecules 23:4582
17. Yang SI, Klein A, Sperling LH (1989) J Polym Sci Part B:Pol Phys 27:1649
18. van den Hul HJ, Vanderhoff JW (1970) Brit Polym 2:121; van den Hul HJ, Vanderhoff JW (1972) J Electroanal Chem 37:161
19. Grunder R, Kim YS, Kranz D, Müller HG, Ballauff M (1991) Angew Chem 103:1715; (1991) Angew Chem Intl Ed 30:1650
20. Grunder R, Urban G, Ballauff M (1993) Colloid Polym Sci 271:563
21. Dingenouts N, Ballauff M (1993) Acta Polymer 44:178
22. Kim YS, Ballauff M (submitted to J Polym Sci:Polym Part A:Polym Chem) Dingenouts N, Kim YS, Ballauff M (1994) Makromol Chem Rapid Comm 15:613
23. Müller HG (1989) Colloid Polym Sci 267:1113
24. Stabinger H, Kratky O (1978) Makromol Chem 179:1655
25. Beniaminy I, Deutsch M (1980) Comp Phys Comm 21:271
26. Strobl GR (1970) Acta Cryst Sect A 26:367
27. Duits MGH, May RP, de Kruif CG (1990) J Appl Cryst 23:336
28. Penders MHGM, Vrij A (1990) Coll Pol Sci 268:823
29. Philipse AP, Smits C, Vrij A (1989) J Coll Int Sci 129:335
30. Helfand E, Tagami Y (1971) Polym Lett 9:741
31. Guinier A, Fournet G (1955) Small Angle Scattering of X-Rays. Wiley, New York
32. Ruland W (1971) J Appl Cryst 4:70
33. Gardon JL (1968) J Polym Sci A6:2859
34. Fisher LW, Polder SM, O'Reilly JM, Ramakrishnan V, Wignall GD (1988) J Coll Interface Sci 123:24

Received April 28, 1994;
accepted May 26, 1994

Authors' address:

Prof. Dr. M. Ballauff
Polymer-Institut der Universität Karlsruhe
Kaiserstraße 12
Postfach 6980
76128 Karlsruhe, FRG